

Statistics on ab-plane offsets in REBCO coated conductors and implications for non-twisted magnets

JL Cheng, Ashleigh Francis, Maise Shepard, Yingtai Chen, Justin Gonzalez, Corey Plant, Catherine Judd, Melanie Russo, Jan Jaroszynski, James Logan, Brian Labombard, Brandon Sorbom

Abstract— The critical current (I_c) of 2G REBa₂Cu₃O_{7-x} (REBCO) high temperature superconductors (HTS) is highly anisotropic with respect to the applied magnetic field (B), with a strong I_c peak expressed at $B \parallel ab$ -plane of the HTS crystal structure. However, as manufactured, there is typically a small-angle ab-plane tilt offset relative to the plane of the tape, and a large average offset can significantly affect magnet I_c if unaccounted for, especially in non-twisted coils such as the SPARC toroidal field magnets being developed by Commonwealth Fusion Systems (CFS). To address this issue, the statistics of the magnitude and orientation of the ab-offset were studied on quick time scales in production quantities for two different HTS vendors by X-Ray Diffraction (XRD) using (005) rocking curves, and the offset was observed to be vendor dependent. The data were correlated positively with offsets determined by SEM, and to I_c at low temperature and moderate to high field by transport and torque magnetometry.

Index Terms— ab-plane offset, critical current, non-twisted HTS magnet, torque magnetometry, X-Ray Diffraction (XRD)

I. INTRODUCTION

COMMONWEALTH Fusion Systems (CFS) is developing a net energy fusion device, SPARC, employing a high field approach (~20 T) enabled by REBCO high temperature superconducting magnets. In the case of non-twisted stacked conductor technology, such as that used in the SPARC toroidal field coils, significant displacement of the angular peak critical current (I_c) at $B \parallel ab$ from the tape plane can significantly reduce operating I_c of the coil. For instance, a 5° I_c peak offset relative to the tape plane results in the actual I_c at the tape plane being as much as 20% less than at the ab-plane location, depending on field and temperature of operation (Fig. 1). At the magnet level, if the stack had a shift in the angular dependence relative to the expected peak location, this would effectively reduce the overall I_c .

This paragraph of the first footnote will contain the date on which you submitted your paper for review, which is populated by IEEE.

This work is supported by Commonwealth Fusion Systems, and a portion of the work was performed at the National High Magnetic Field Laboratory, which is supported by National Science Foundation Cooperative Agreement No. DMR-1644779, DMR-212855, UCGP and the State of Florida. (*Corresponding author: JL Cheng*).

JL Cheng, Ashleigh Francis, Maise Shepard, Yingtai Chen, Justin Gonzalez, Corey Plant, Catherine Judd, Melanie Russo, James Logan, and Brandon Sorbom are with Commonwealth Fusion Systems, Devens, MA 01434 USA (e-mail: jcheng@cfs.energy; afrancis@cfs.energy; msheward@cfs.energy; ychen@cfs.energy; jgonzalez@cfs.energy; crp2709@rit.edu; cjudd@cfs.energy; mr3551@columbia.edu; jlogan@cfs.energy; bsorbom@cfs.energy).

Jan Jaroszynski is with National High Field Magnet Laboratory, Tallahassee, 32310 USA. (e-mail: jaroszy@magnet.fsu.edu).

Brian Labombard is with Massachusetts Institute of Technology Plasma Science and Fusion Center, Cambridge MA, 02139 USA (e-mail: labombard@psfc.mit.edu).

Color versions of one or more of the figures in this article are available online at <http://ieeexplore.ieee.org>

Transport measurements taken on a Supercurrent measurement system (Fig. 2) show that I_c peak varies as a function of (B, T, θ). This is likely due to the transition to intrinsic pinning at high fields [1] [2]. Detailed characterization of $I_c(\theta)$ and the statistics of the magnitude and orientation of the angular offset of the ab-plane is important for the design and operation of SPARC coils. For the high throughput needed on a commercial scale, such angular characterization would ideally be rapid, non-destructive, and repeatable, with correlation to transport measurements.

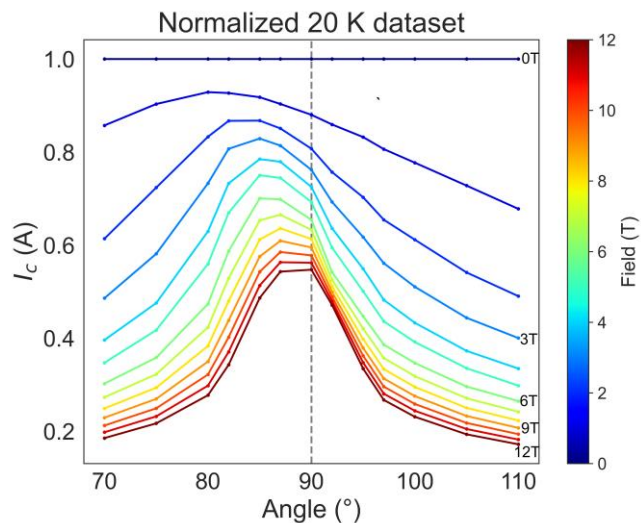


Fig. 1. Normalized $I_c(\theta)$ at 20 K, 0-12 T in 1 T steps, shows the sensitivity of I_c close to 90°; small offsets can affect I_c at 90° significantly.

3MOr1B-06

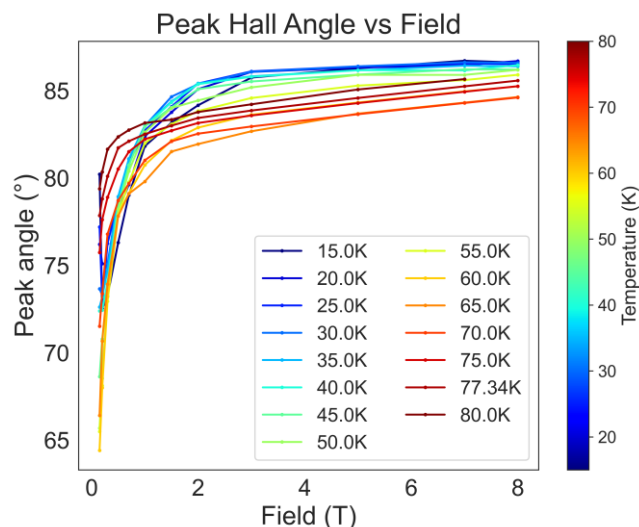


Fig. 2. Peak transport Hall sensor angle vs Field from 15-80 K, showing shift in peak angle as a function of field and temperature

Previous work has shown that the ab-plane offset originates in the IBAD-MgO buffer layer and suggested that rotating the orientation of IBAD deposition to the lengthwise direction may eliminate the ab-plane offset [3]. The same study also investigated the statistics of the ab-tilt of Superpower tapes using XRD in the context of magnet design and construction, demonstrating a small but consistent positive average offset, with a mean of 2.2° and standard deviation of 0.5° for 68 samples. The consistency of the tilt magnitude and direction along ~ 20 m length conductors from three commercial vendors has also been investigated, showing that lengthwise homogeneity is highly vendor dependent [4]. Additionally, strong correlations between reel-to-reel XRD data and self- and in-field PPMS performance have been demonstrated with a 2D inline XRD system [5]. This further suggests that XRD is a valuable tool for the rapid qualification of long lengths of HTS.

This study seeks to characterize the statistics of such offsets in production quantities for two vendors, correlate the results to SEM, transport, and torque measurements, and apply the results to an EM model to investigate the impact of offset angle on operating I_c .

II. EXPERIMENT

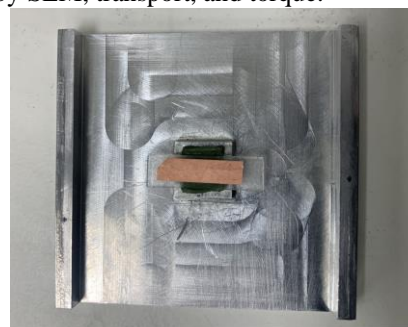
A. Sample details

HTS samples from reels of two vendors, “F” and “H”, were measured for this study. For all samples, the nominal Cu layer thickness was $5 \mu\text{m}$, with the Ag layer nominally $2\text{-}3 \mu\text{m}$. The original orientation of the sample relative to the reel position was tracked using cuts on the corners of the samples, which were consistently oriented for each measurement type.

A. XRD Measurements

(005) rocking curves were taken using a Bruker AXS Smart Apex system with Cu $K\alpha$ $\lambda=1.54 \text{ \AA}$ at 0.2 seconds per 0.05° step for $\theta=14\text{-}24^\circ$. This rate allowed each sample measurement scan to be completed in about 1 minute, not including the

comparable amount of time required for sample mounting. 16 samples from vendor F reels and 359 samples from vendor H reels representing three magnet test coils were measured with the Cu layer etched off, leaving a nominal $3 \mu\text{m}$ Ag layer over the REBCO layer. Samples were cleaned and double-sided taped to a thin glass slide. The slide and sample were then placed on the mounting stage, which is topped with a soft green putty (Fig. 3a). The sample, slide, and putty are then pressed flat using a glass block. (Fig. 3b) Ab-plane offsets determined using such rocking curves are later correlated to offsets determined by SEM, transport, and torque.



(a)



(b)

Fig. 3. (a) Sample with cut corner mounted on slide and placed over putty (b) sample press-aligned flat relative to edges of mounting block using a glass block

To quantify the repeatability of the measurement method, rocking curves for a separate set of H and F samples were measured multiple times, with samples unmounted and remounted between tests. For the repeatability study, five samples were taken along the length of one reel from each vendor (Fig. 4). These two reels are referred to as H1 and F1. Five samples from each of five other reels by vendor H, labeled H51, H63, H67, H88, and H100, were also studied. Each of these samples was measured first with Cu layer intact, then chemically etched such that Ag layer and then the REBCO layer were exposed (Table 1). Two trials were run with the Cu layer to evaluate the necessity of performing optimization of intensity in the ϕ and χ axes.

3MOr1B-06

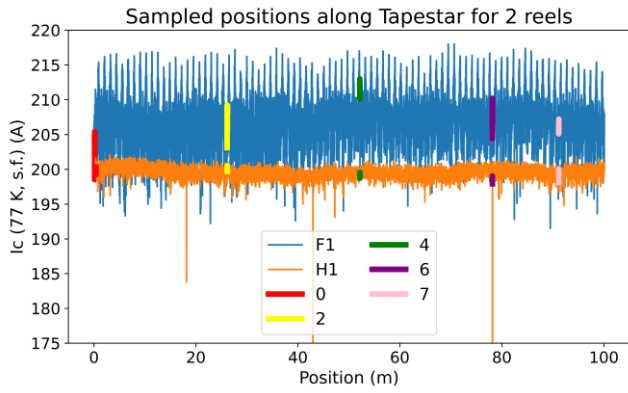


Fig. 4. Numbered sample positions (0, 2, 4, 6, and 7) for F1 and H1 reels, where the number indicates the nth hundred sample, i.e. 2 is the 200th 13 cm sample of 770 samples along 100 m

TABLE 1

SUMMARY OF REPEATABILITY STUDY MEASUREMENTS

Layer	$\phi\chi$ optimize	F samples	F tests / sample	H samples	H tests / sample
Cu (1)	Y	5	5	5	5
Cu (2)	N	5	5	5	5
Ag	N	5	5	10	5
ReBCO	N	3	5	3	5

B. SEM imaging

29 H samples and nine F samples were etched down to the REBCO layer and imaged using a Phenom Pharos G2 SEM at 15000X-16000X magnification to confirm the relative tilt direction of the REBCO in reference to the tracked reel position.

C. Transport Measurements

28 H samples and 14 F samples were tested at 4.5 cm length x 4 mm width using a Supercurrent measurement system [6] at 77 K, 0.25 T, 0-180°. An additional nine H samples and four F samples were laser bridged to 0.4 mm and 0.15 mm width respectively for 20 K measurements at 12 T and 0-180°. The laser system used was a Wedge XF 532 operating at 90W 200 mm/s 50 kHz and 90 passes. All samples were measured with the Cu layer intact and soldered to current contacts and 10 mm voltage taps at below 160 °C with InBi solder. I_c was determined using the 1 μ V/cm electric field criterion. The angular orientation was confirmed by a pair of perpendicular hall effect sensors mounted at the sample location.

D. Torque Measurements

The angular dependence of $I_c(B, T)$ was measured at 20 K, 6-25 T, and angles 30-150° for four H samples and three F samples at the NHMFL in a 31 T resistive magnet using torque magnetometry [7]. Because the sample is constantly rotating during this form of measurement, the angular orientation of the sample was confirmed using a pickup coil. Sample dimensions were 4 mm x 1.3 cm, and the Cu layer for all samples was intact.

III. RESULTS AND DISCUSSION

A. XRD Results

The ab-plane offsets were determined as the difference between the angle at the curve peak as fit with a pseudo-Voigt curve using Jade MDI software and the nominal $\theta = 19.256^\circ$ for (005) plane [8]. Characteristic rocking curves for the repeatability study (Fig. 5) show that the precision of the measurement depends on the shape and fit of the curve and that etching down to the REBCO layer improves signal to noise ratio but does not show consistent trends for peak direction shift.

The overall results (Fig. 6) are summarized by the mean, standard deviation (STDEV), and 95% confidence intervals in Table 2, where the HX grouping refers to the 5 vendor H samples from H51, H63, H67, H88, and H100.

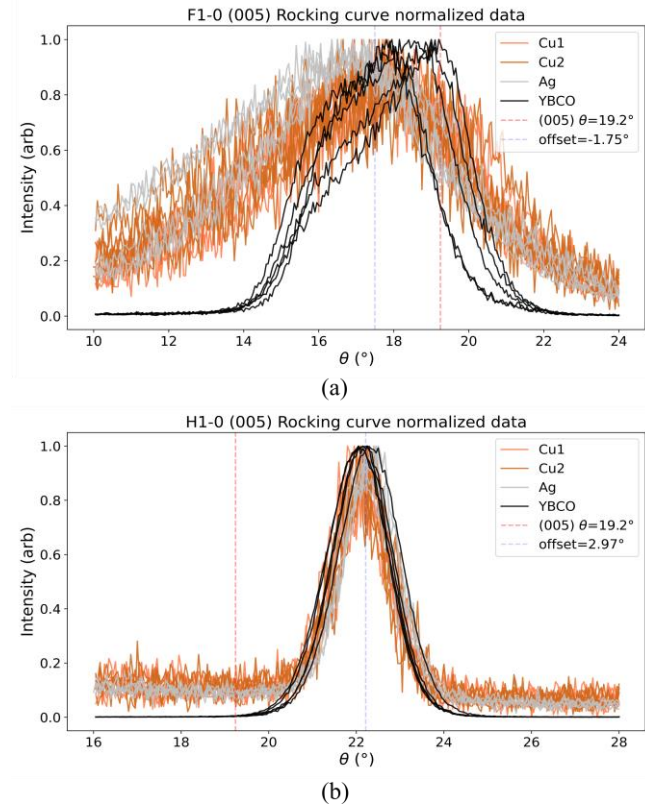


Fig. 5. Overlain (005) rocking curves for (a) F1-0 sample and (b) H1-0 sample

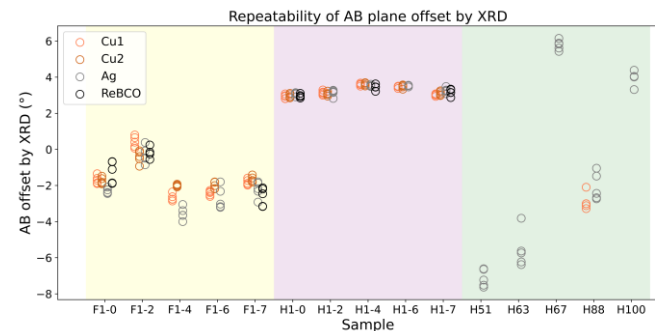


Fig. 6. AB-plane offset measurement results for each sample in repeatability study

3MOr1B-06

TABLE 2

AB-PLANE OFFSET STATISTICS IN REPEATABILITY STUDY

Group	Mean	STDEV	95% CI
F1	-1.81	0.53	0.49
H1	3.25	0.11	0.11
HX	-1.09	0.58	0.94

359 H samples were measured using the same rocking curve method (Fig. 7). The results show a bimodal distribution with a higher tendency towards positive offsets over time, indicating that the manufacturer may have standardized their respooling orientation.

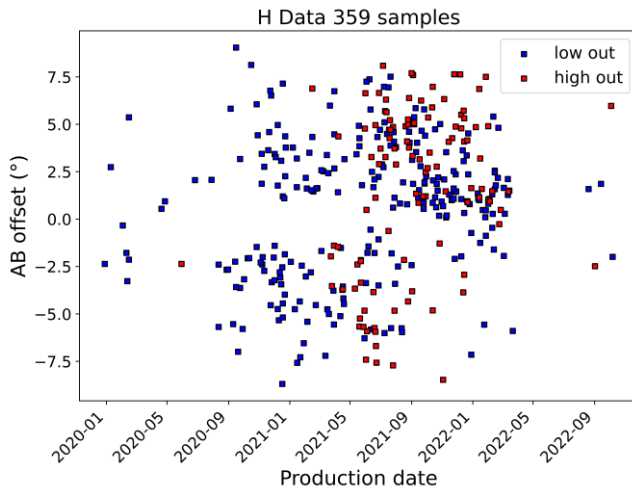
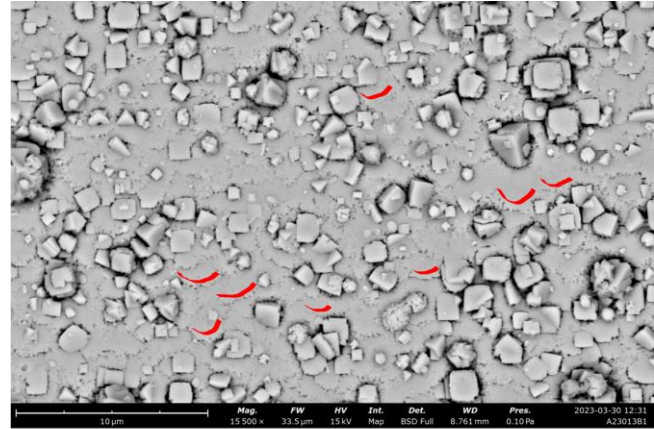


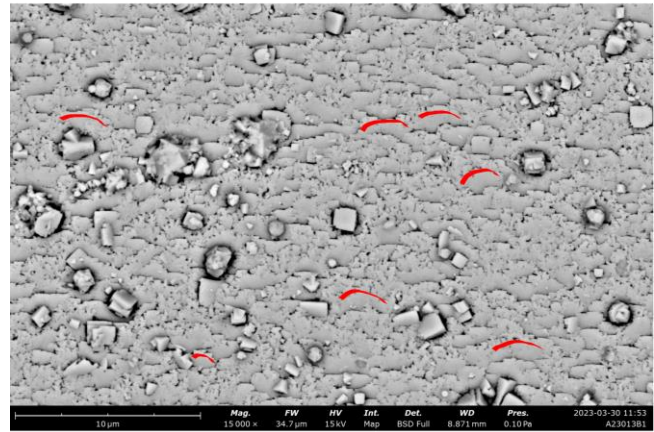
Fig. 7. AB-plane offset measurement results for 359 H samples, color coded by orientation of high meter marking by Tapestar data relative to outer diameter position

B. SEM Imaging

SEM images were taken for 38 samples, of which 29 were H samples and nine were F samples. For samples without highly disordered surfaces, the background grain pattern is distinguishable. It was observed that grains for most H samples were tilted, appearing much like the scales of a fish (Fig. 8). Based on the direction or lack of direction of the grain tilts, the images could be categorized as “left”, “neutral”, or “right” relative to the tracked reel position. Although the categories are not quantitative, qualitatively it can be observed that the right tilt in Fig. 8b is likely of larger magnitude than the left tilt of Fig. 8a, based on the more dramatic shadows. The categorization of samples was consistent with the orientation predicted by XRD measurements, further validating the XRD measurements (Fig. 9). It is possible that with intelligent image processing, tilts could be quantified, although for this purpose XRD is more practical. For two measured samples, the REBCO surface was too disordered to determine the orientation, and these were therefore categorized as “disordered”. It is notable that H samples tended to be either left or right oriented, while F samples tended to be neutral. Samples with ab-plane offsets greater than +2° or less than -3° were consistently identified correctly by SEM. Results are tabulated in Table 3.



(a)



(b)

Fig. 8. (a) An example of a “left” oriented sample; the flake-like grains, with a few example edges outlined in red, tilt up at the bottom, as can be seen by the shadow-like areas at the lower grain boundary (b) An example of a “right” oriented sample with the grains tilting up at the top.

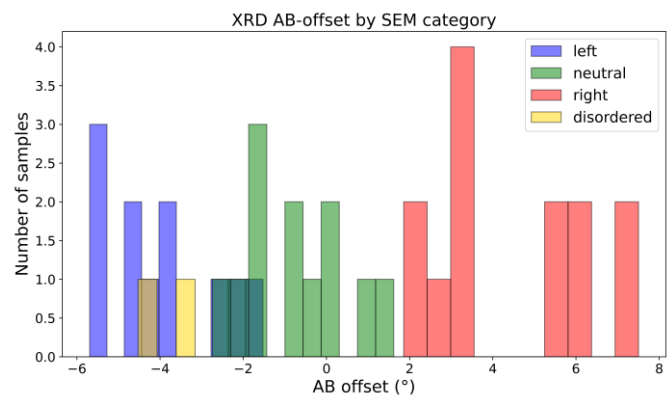


Fig. 9. Histogram of SEM category by XRD AB offset

TABLE 3

SEM ORIENTATION CATEGORY

	Left	Neutral	Right	Disordered
Total Count	11	12	13	2
Total offset Mean	-3.96	-0.75	4.42	-3.84

3MOr1B-06

H Count	10	4	13	2
F Count	1	8	0	0

C. Transport Results

The I_c peak angle for each angular dependence was determined by taking the maximum value after applying a smoothing filter, with the ab-plane offset being the difference between the peak angle and 90° . Transport offsets are plotted against XRD offsets in closed face circles for vendor H and open face circles for vendor F (Fig. 10). Pearson correlation coefficients and corresponding p-values indicating the probability the Pearson coefficient could have been drawn from a random distribution (Table 4) were calculated, showing high correlation for H samples. Like for the SEM and XRD results, the magnitudes of offsets were higher for H samples, contributing to improved correlations. Therefore, for only H samples, the slope, intercept, and R^2 have also been calculated for linear regression.

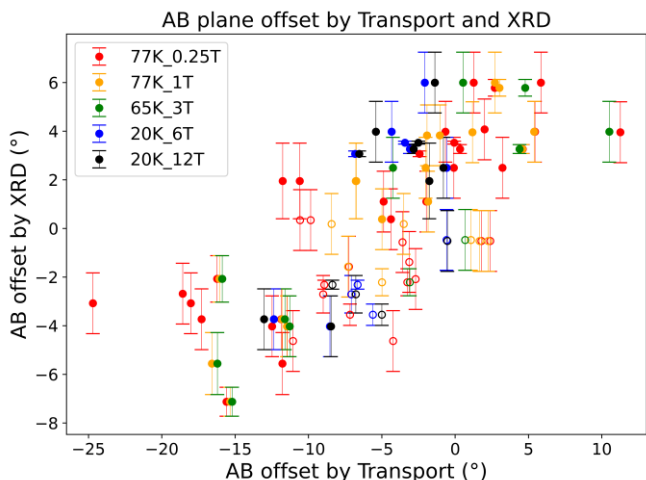


Fig. 10. AB offsets by XRD vs Transport

TABLE 4

AB-PLANE OFFSET STATISTICS IN REPEATABILITY STUDY

	77K_0.25T	77K_1T	65K_3T	20K_6T	20K_12T
	full width 4mm wide sample			0.15-0.4 mm bridge	
F count	14	7	2	4	4
F Pearson	0.22	0.18	-	0.83	0.68
F p-val	0.44	0.70	-	0.17	0.32
H count	28	17	10	8	9
H Pearson	0.84	0.91	0.89	0.82	0.79
H p-val	0.00	0.00	0.00	0.01	0.01
H slope	0.35	0.5	0.44	0.78	0.67
H intercept	2.65	3.27	2.29	5.83	5.03
H R^2	0.7	0.83	0.79	0.67	0.63

D. Torque Results

I_c peak angle was calculated from the force measured by load cell as the samples were rotated in field. The peak angle shows a similar trend with XRD determined ab-offsets, however the correlation is negative here because the sample orientation for

torque measurements is flipped relative to transport and XRD orientation (Fig. 11).

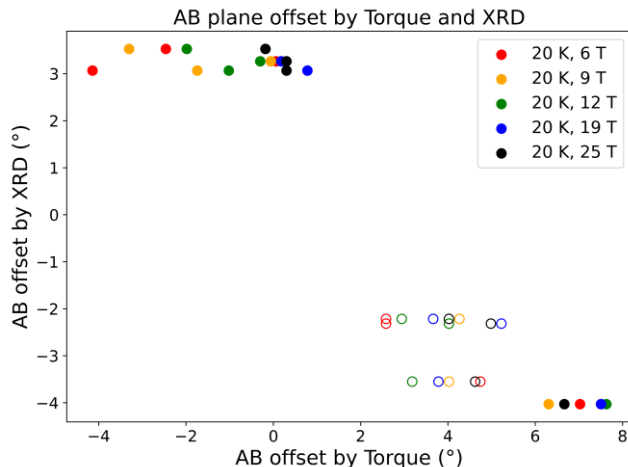


Fig. 11. AB-plane offset by XRD vs Torque

E. Application to Magnet modeling

Of the 359 XRD ab-plane offset measurements, 355 represent samples from reels of three magnet test coils (Fig. 12). Applying the 77 K, 1 T slope and intercept (Table 4) to convert from XRD to transport offset, the equivalent shifts at 77 K, 1 T for a transport dataset can be determined (Table 5). Such offset shifts can be applied to $I_c(B, T, \theta)$ design dataset tables, used as inputs to critical current estimation models to determine the impact of I_c if the offset is not controlled in the stack.

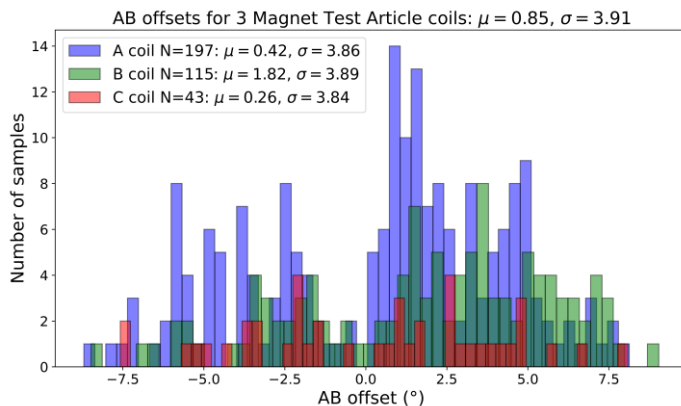


Fig. 12. Histogram of XRD AB-plane offsets for 3 test coils

TABLE 5

SUMMARY OF OFFSETS FOR 3 MAGNET TEST ARTICLES

Test Article	Reels tested	% tested	Mean XRD offset	Margin of error	77K 1T offset
A	197	100%	0.42	0%	-5.7
B	115	57.5%	1.82	6%	-2.9
C	43	21.39%	0.26	13%	-6.02

Although it is known that I_c of HTS varies along its length due to non-uniform manufacturing, for the purpose of this model, the stack is assumed to use the same table along the length. This is justified based on tape selection of the stack to avoid sections with significant variations in I_c . The other inputs

3MOr1B-06

to the model are the I_c and thicknesses of tapes used in the coil, used to scale the dataset tables appropriately, and the geometry of the coil and HTS stack (Fig. 13). With these inputs, the three test coils were modeled using a steady state critical current estimator model. The model breaks down the HTS stack into a grid of current carrying filaments (Fig. 14) at the point of interest along the arclength of the coil. It then calculates Biot-Savart at evaluation points in the grid for each filament and superimposes the field from the filaments. The solver iteratively raises current and solves for field until critical criterion ($I_{op} = I_c$) is reached based on input data at the point of interest. The point of interest is swept along the arclength of the coil and coil I_c is then taken as the minimum I_c along the arclength of the coil.

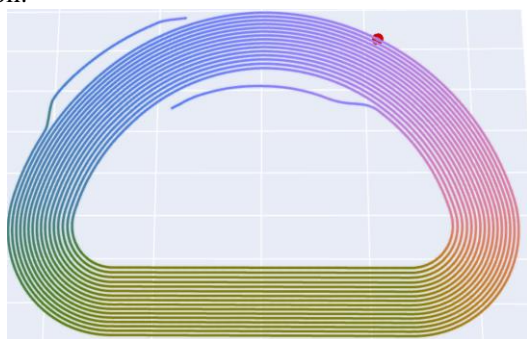
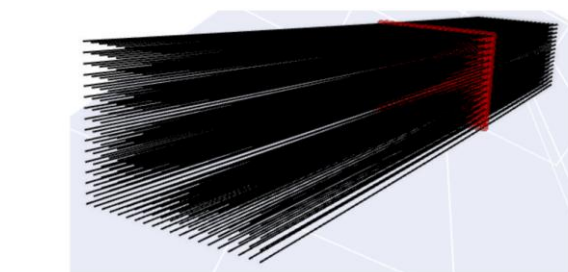


Fig. 13. Geometry of HTS stack in test coils, with evaluation point shown as red dot, swept along the arclength of the coils.



Stack B Total [T]

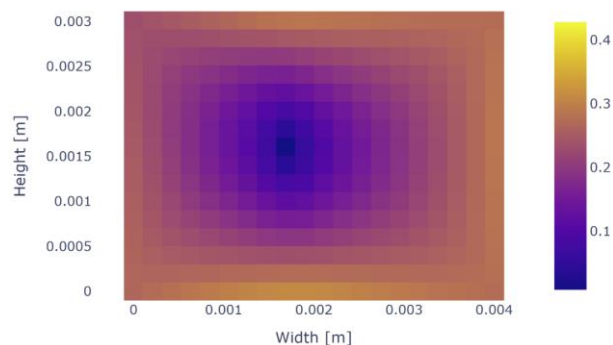


Fig. 14. Current carrying filaments form a grid representing the geometry of the stack, with the point of interest along the length of the filaments shown in red. The stack field map determined by the method at $I_c(77\text{ K, self-field})$ is shown at the point of interest

Coil I_c for test article A, B, and C for the 77 K, 1 T offset cases, normalized to the symmetric case, was computed at 77 K

and 20 K (Table 6), demonstrating that the result is significantly more sensitive to offsets at low temperature, high field.

TABLE 6

I_c RELATIVE TO SYMMETRIC CASE FOR 3 TEST MAGNETS

Test Article	Relative I_c 20 K	Relative I_c 77 K
Symmetric	1.00	1.00
A	0.958	0.989
B	0.965	0.994
C	0.957	0.989

V. CONCLUSION

Rapid nondestructive XRD (005) rocking curve measurements were shown to be repeatable and highly correlated with grain orientation via SEM as well as with the I_c peak offset from transport and torque measurements. Such qualities suggest that XRD rocking curve measurements can be used effectively in the quality assurance of large volumes of HTS for applications such as fusion magnets for additional insight into ab-plane offset statistics.

Additionally, measured statistics for ab plane offsets varied significantly by manufacturer, with larger offsets for vendor H than vendor F. Modeling a test coil with data offset as predicted by measured statistics and correlation with transport data shows very small effect of peak offset on I_c performance at 77 K and more significant effect on I_c performance at 20 K.

REFERENCES

- [1] L. Civale *et al.*, "Identification of intrinsic ab-plane pinning in YBa₂Cu₃O₇ thin films and coated conductors," *IEEE Trans. Appl. Supercond.*, vol. 15, no. 2, Art. no. 2, Jun. 2005, doi: 10.1109/TASC.2005.848218.
- [2] B. Maiorov, B. J. Gibbons, S. Kreiskott, V. Matias, T. G. Holesinger, and L. Civale, "Effect of the misalignment between the applied and internal magnetic fields on the critical currents of 'tilted coated conductors,'" *Appl. Phys. Lett.*, vol. 86, no. 13, Art. no. 13, Mar. 2005, doi: 10.1063/1.1886253.
- [3] J. Lu, Y. Xin, Y. Zhang, and H. Bai, "ab-Plane Tilt Angles in REBCO Conductors," *IEEE Trans. Appl. Supercond.*, vol. 33, no. 5, Art. no. 5, Aug. 2023, doi: 10.1109/TASC.2023.3236258.
- [4] J. Lee, "Lengthwise Characterization of Crystallographic Tilt in Contemporary REBCO Coated Conductors," presented at the Applied Superconductivity Conference, Salt Lake City, UT, Sep. 2024.
- [5] S. Chen *et al.*, "Scale Up of High-Performance REBCO Tapes in a Pilot-Scale Advanced MOCVD Tool With In-Line 2D-XRD System," *IEEE Trans. Appl. Supercond.*, vol. 31, no. 5, pp. 1–5, Aug. 2021, doi: 10.1109/TASC.2021.3058868.
- [6] N. M. Strickland *et al.*, "Extended-Performance 'SuperCurrent' Cryogen-Free Transport Critical-Current Measurement System," *IEEE Trans. Appl. Supercond.*, vol. 31, no. 5, pp. 1–5, Aug. 2021, doi: 10.1109/TASC.2021.3060355.
- [7] J. Jaroszynski *et al.*, "Rapid assessment of REBCO CC angular critical current density $J_c(B, T = 4.2\text{ K}, \theta)$ using torque magnetometry up to at least 30 tesla," *Supercond. Sci. Technol.*, vol. 35, no. 9, p. 095009, Aug. 2022, doi: 10.1088/1361-6668/ac8318.
- [8] W. Wong-Ng *et al.*, "Standard X-Ray Diffraction Powder Patterns of Sixteen Ceramic Phases," *Powder Diffr.*, vol. 2, no. 3, pp. 191–202, Sep. 1987, doi: 10.1017/S0885715600012690.